

Boundary Perturbation Effects in Quantum Systems with Conserved Energy and Continuous Symmetry

Qucheng Gao^{1,*} and Xiao Chen^{1,†}

¹*Department of Physics, Boston College, Chestnut Hill, Massachusetts 02467, USA*

We investigate one-dimensional systems with both energy conservation and a continuous symmetry, focusing on the impact of a boundary perturbation that breaks the continuous symmetry. Our study examines the quantum dynamics resulting from this boundary perturbation and identifies two distinct phases: one in which the corresponding charge exhibits extensive fluctuations, and another where the charge remains conserved. These phenomena are observed in both free and interacting models. The emergence of the charge-frozen phase is attributed to energy conservation, and we demonstrate that this phase disappears when energy conservation is broken or replaced by other symmetries. We provide an explanation using the effective Hamiltonian derived from degenerate perturbation theory.

CONTENTS

I. Introduction	1
II. Boundary perturbation on a free-fermion chain	2
III. Boundary perturbation on an interacting fermionic chain	2
IV. Boundary perturbation on an interacting spin chain	3
V. Effective Hamiltonian	4
VI. Boundary perturbation on Floquet systems	6
VII. Discussion	6
Acknowledgments	7
References	7
A. Particle dynamics and energy dynamics of free-fermion chain	A1
B. Interacting fermionic chain with a filling factor $\nu = 0.25$	A1
C. Derivation of the effective Hamiltonian	A1
D. Particle transport in a free-fermion chain	A2

I. INTRODUCTION

The influence of a single impurity on a many-body system presents a fascinating and fundamental question. One particularly well-known example is the Kondo effect,

where a magnetic impurity can dramatically alter the transport properties of a metal at low temperatures [1, 2]. This phenomenon has been further interpreted through the lens of boundary conformal field theory [3, 4].

Beyond this, similar setups have been explored in the context of highly non-equilibrium dynamics induced by boundary perturbations. These studies span both classical stochastic processes [5] and quantum systems [6]. Recently, such setups have also been investigated from the perspective of quantum information [7, 8]. Remarkably, it was found that a single interaction term can induce the scrambling of information across the entire free-fermion random circuit system in low dimensions. However, in three dimensions, tuning the strength of the impurity induced a scrambling phase transition [8].

Building on previous work, this paper investigates a one-dimensional quantum *Hamiltonian* system with a global $U(1)$ symmetry, which ensures the conservation of the total charge. We add a boundary perturbation to the Hamiltonian that explicitly breaks the $U(1)$ symmetry and address the following question: How does the charge in the bulk evolve in the presence of this boundary perturbation?

At first glance, one might expect the boundary perturbation to allow charge to flow into or out of the system, leading an initial state with a fixed charge to evolve into a superposition of states spanning multiple charge sectors. This expectation holds in systems without energy conservation, such as those governed by driven dynamics or quantum circuit models, where thermalization across the entire Hilbert space can occur. However, in our system, the dynamics are governed by Hamiltonian evolution, which conserves the total energy. As we demonstrate in this paper, the interplay between boundary perturbations and energy conservation results in more intricate behavior. By varying the parameters in the bulk of the system, we uncover two distinct phases: in one phase, charge fluctuations are negligible, and the total charge remains nearly conserved, with only an $O(1)$ change; in the other, significant charge fluctuations arise, allowing the total average charge to vary dramatically.

The existence of the charge-frozen phase arises from

* gaoqc@bc.edu

† chenaad@bc.edu

energy conservation, which constrains the free movement of charge into or out of the bulk. This behavior can be simply understood as follows: moving charge into or out of the system requires additional energy, which is forbidden under strict energy conservation. We substantiate these findings with numerical results for free and interacting fermionic systems (Sec. II and Sec. III), and interacting spin systems (Sec. IV). We propose a criterion for the phase transition using the effective Hamiltonian derived from degenerate perturbation theory (Sec. V). We also demonstrate that the energy conservation is a necessary condition for the existence of the phase transition (Sec. VI). We summarize our results in Sec. VII.

II. BOUNDARY PERTURBATION ON A FREE-FERMION CHAIN

We start with a one-dimensional free-fermion chain of finite size L with periodic boundary condition (PBC). The Hamiltonian is

$$\begin{aligned}\hat{H}_0 &= \sum_{j=1}^L t_0 (\hat{c}_j^\dagger \hat{c}_{j+1} + \hat{c}_{j+1}^\dagger \hat{c}_j) - \sum_{j=1}^L \mu_0 \hat{n}_j \\ &= \sum_k (2t_0 \cos k - \mu_0) \hat{c}_k^\dagger \hat{c}_k,\end{aligned}\quad (1)$$

where \hat{c}_j is the annihilation operator of the fermion on site j , $\hat{n}_j \equiv \hat{c}_j^\dagger \hat{c}_j$, t_0 is the hopping parameter, and μ_0 is the chemical potential. The second equality utilizes the Fourier transform $\hat{c}_j = \frac{1}{\sqrt{L}} \sum_k e^{ikj} \hat{c}_k$. For simplicity, we assume $t_0 > 0$ throughout. Note that \hat{H}_0 commutes with the number operator $\hat{N} = \sum_j \hat{n}_j$ and therefore the total particle number is conserved. We prepare our system $|\Psi(0)\rangle$ of \hat{N} with a fixed particle number N , i.e.,

$$\hat{N} |\Psi(0)\rangle = N |\Psi(0)\rangle. \quad (2)$$

At time $t = 0$, we introduce a boundary perturbation \hat{H}_B ,

$$\begin{aligned}\hat{H}_B &= \Delta (\hat{c}_1^\dagger \hat{c}_2^\dagger + \hat{c}_2 \hat{c}_1) \\ &= \frac{\Delta}{L} \sum_{k_1 k_2} \left(e^{-i(k_1+2k_2)} \hat{c}_{k_1}^\dagger \hat{c}_{k_2}^\dagger + e^{i(k_1+2k_2)} \hat{c}_{k_2} \hat{c}_{k_1} \right),\end{aligned}\quad (3)$$

which does not commute with \hat{N} . For times $t > 0$, the state of the system evolves as

$$|\Psi(t)\rangle = e^{-i\hat{H}t} |\Psi(0)\rangle, \quad (4)$$

where $\hat{H} = \hat{H}_0 + \hat{H}_B$. In this setup, the boundary perturbation can disrupt particle number conservation during time evolution. Our goal is to investigate *how the boundary perturbation affects the initially conserved quantity in the bulk*. To quantify the changes in the initially conserved particle number, we analyze the charge variance:

$$\delta N^2(t) = \langle \Psi(t) | (\hat{N} - \langle \Psi(t) | \hat{N} | \Psi(t) \rangle)^2 | \Psi(t) \rangle. \quad (5)$$

The quadratic Hamiltonian and the Gaussian free-fermionic state allow for efficient simulations on classical computers [9, 10]. We prepare a randomly filled product state with a filling factor ν , ensuring that initial state has $N = L\nu$. This state is evolved for a long time with $t = 2L$, and the steady-state value of δN^2 is computed as a function of μ_0 (see also Appendix A for the particle dynamics and energy dynamics). The results for various system sizes L are shown in Fig. 1(a) and Fig. 1(b). We observe a phase transition at $|\mu_0| = 2t_0$. When $|\mu_0| > 2t_0$, the boundary perturbation induces only an $O(1)$ change in the charge in the thermodynamic limit. This is evident in Fig. 1(b), where $\delta N^2(t = 2L)$ remains a small finite value across different system sizes. On the other hand, when $|\mu_0| < 2t_0$, there are strong charge fluctuations with $\delta N^2(t = 2L)$ proportional to the system size L . This behavior indicates that the final state is an extensive superposition of wavefunctions with different charge sectors. Note that, in the free fermion model, the phase transition point coincides with the gap closing point of the single-particle spectrum. We will give an explanation of this behavior later in Sec. V. The phase transition can also be observed from the charge difference between the final state and the initial state:

$$\delta N(t) = \langle \Psi(t) | \hat{N} | \Psi(t) \rangle - \langle \Psi(0) | \hat{N} | \Psi(0) \rangle. \quad (6)$$

As shown in Fig. 1(c), when $|\mu_0| < 2t_0$, the charge undergoes significant changes unless the initial state is exactly at half-filling. In contrast, when $|\mu_0| > 2t_0$, the charge changes by at most an $O(1)$ constant in the presence of boundary perturbations.

III. BOUNDARY PERTURBATION ON AN INTERACTING FERMIONIC CHAIN

To investigate whether the above phenomena persist in an interacting system, we now consider a simple interacting model by adding an interaction term to the original free \hat{H}_0 . The new \hat{H}_0 becomes

$$H_0 = \sum_{j=1}^L t_0 (\hat{c}_j^\dagger \hat{c}_{j+1} + \hat{c}_{j+1}^\dagger \hat{c}_j) - \sum_{j=1}^L \mu_0 \hat{n}_j + \sum_{j=1}^L U \hat{n}_j \hat{n}_{j+1}. \quad (7)$$

The boundary term \hat{H}_B remains unchanged. We prepare a randomly filled product state with a filling factor of $\nu = 0.5$ and study the charge fluctuations in the presence of a boundary perturbation. Numerical results for other filling factors are provided in Appendix B. We fix $U = 2$ and compute $\delta N^2(t = 2L)$ as a function of μ_0 . Since the system is no longer a free fermion dynamics, we simulate its dynamics using exact diagonalization for small system sizes. Results for different system sizes L are shown in Fig. 2(a) and Fig. 2(b), where a similar phase transition is observed. The charge fluctuation is extensive for $-2 \lesssim \mu_0 \lesssim 6$ and negligible outside this range.

We can also fix $\mu_0 = 4$ and vary the interaction strength U . As shown in Fig. 2(c) and Fig. 2(d), the

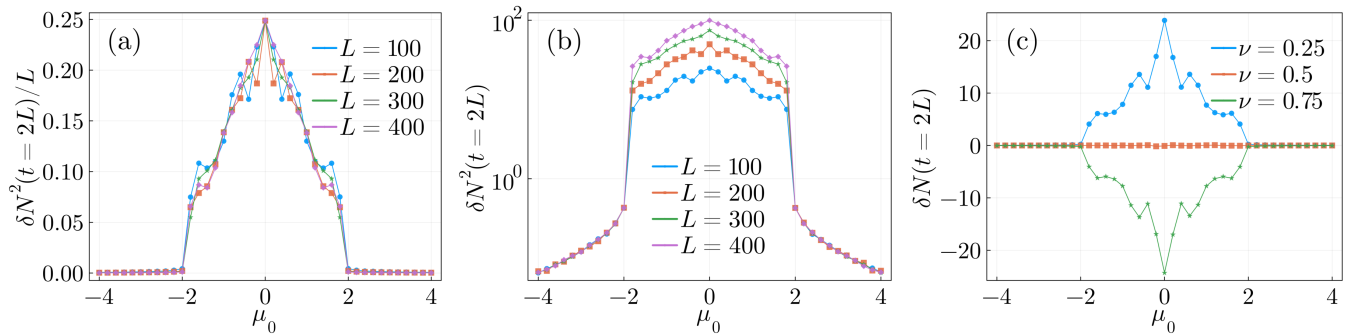


FIG. 1. Free-fermion chain. (a) The density of charge variance $\delta N^2/L$ as a function of μ_0 for different system sizes. (b) The charge variance δN^2 as a function of μ_0 for different system sizes on a log-lin scale. Here, $t_0 = \Delta = 1$, $\nu = 0.5$, and the results are averaged over 1000 samples. (c) The charge difference δN as a function of μ_0 for different filling factors. Note that when the initial state is at half-filling, the charge difference is unable to detect the phase transition. Here, $t_0 = \Delta = 1$, $L = 100$, and the results are averaged over 1000 samples.

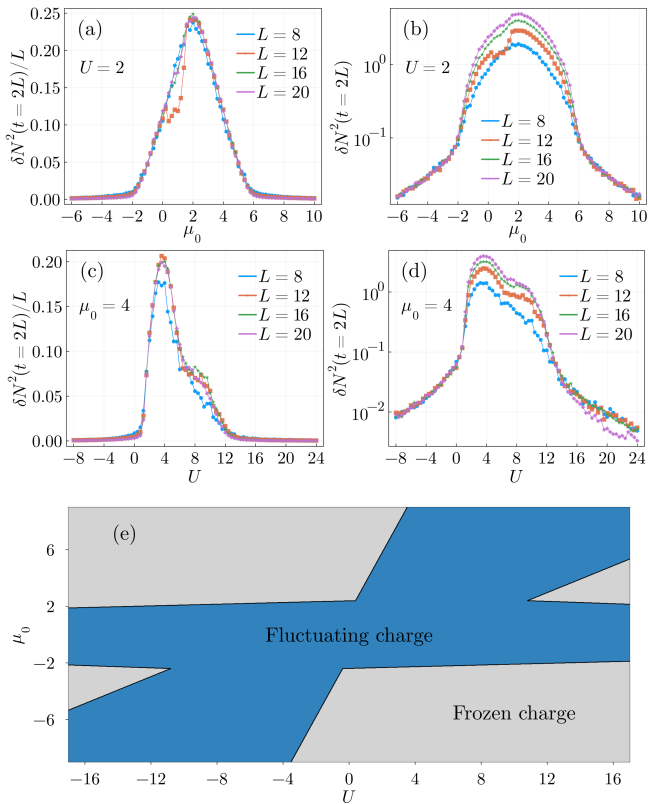


FIG. 2. Interacting fermionic chain. (a) The density of charge fluctuation $\delta N^2/L$ as a function of μ_0 for different system sizes. (b) The charge variance δN^2 as a function of μ_0 for different system sizes on a log-lin scale. Here, $t_0 = \Delta = 1$, $U = 2$, $\nu = 0.5$, and the results are averaged over 200 samples. [(c) and (d)] Same as (b) and (c), but with $\mu_0 = 4$ fixed and U varied. (e) Two-dimensional phase diagram of μ_0 and U . The blue region represents extensive charge fluctuation and is labeled as “Fluctuating charge”. The gray region represents negligible charge fluctuation and is labeled as “Frozen charge”.

results for $\mu_0 = 4$ indicate that the charge fluctuation is extensive for $1 \lesssim U \lesssim 14$ and negligible outside this range. We also extract a two-dimensional phase diagram by varying μ_0 and U , as shown in Fig. 2(e). It is important to note that the phase boundary may not be entirely accurate and is likely subject to strong finite-size effects due to system size limitations. However, at $U = 0$, the phase boundary is approximately consistent with results obtained from larger systems in the previous section.

IV. BOUNDARY PERTURBATION ON AN INTERACTING SPIN CHAIN

We consider an interacting spin chain of finite size L with PBC. The bulk Hamiltonian is

$$\hat{H}_0 = \sum_{j=1}^L \left(J^x (\hat{\sigma}_j^x \hat{\sigma}_{j+1}^x + \hat{\sigma}_j^y \hat{\sigma}_{j+1}^y) + J^z \hat{\sigma}_j^z \hat{\sigma}_{j+1}^z \right) + \sum_{j=1}^L h \hat{\sigma}_j^z, \quad (8)$$

and the boundary perturbation is

$$\hat{H}_B = \Delta \hat{\sigma}_1^x. \quad (9)$$

Here, $\hat{\sigma}_j^\alpha$ denote Pauli matrices at different lattice sites j with $\alpha = x, y, z$. The bulk Hamiltonian \hat{H}_0 is the XXZ spin chain in a magnetic field. Note that \hat{H}_0 commutes with the spin operator $\hat{S}^z = \frac{1}{2} \sum_j \hat{\sigma}_j^z$, so that the total S^z is conserved. The boundary term \hat{H}_B explicitly breaks this conservation law. We prepare the initial state $|\Psi(0)\rangle$ of \hat{S}^z with a fixed S^z , i.e.,

$$\hat{S}^z |\Psi(0)\rangle = S^z |\Psi(0)\rangle. \quad (10)$$

For times $t > 0$, the system evolves unitarily with $\hat{H} = \hat{H}_0 + \hat{H}_B$, and we analyze the spin variance in the z -direction:

$$\delta S^{z^2}(t) = \langle \Psi(t) | (\hat{S}^z - \langle \Psi(t) | \hat{S}^z | \Psi(t) \rangle)^2 | \Psi(t) \rangle. \quad (11)$$

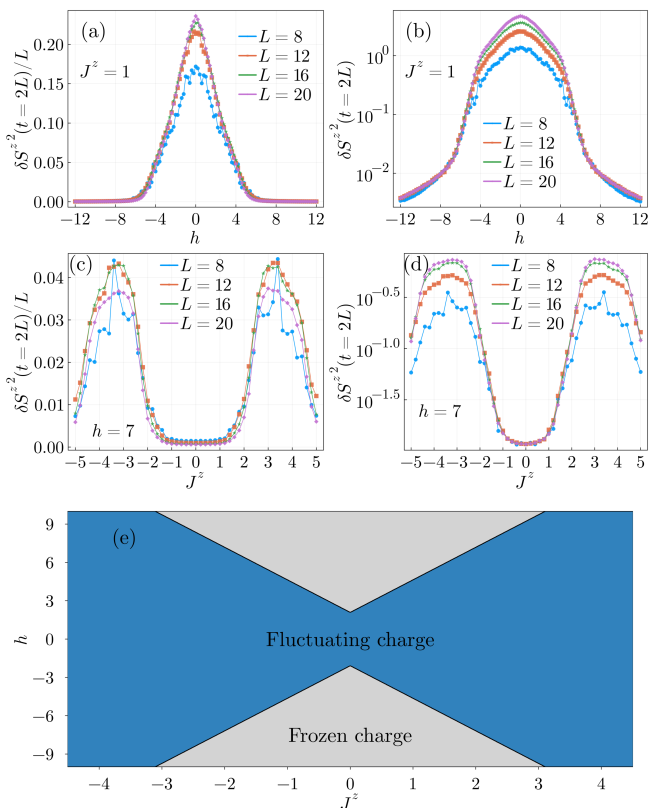


FIG. 3. Interacting spin chain. (a) The density of charge fluctuation $\delta S^{z^2}/L$ as a function of h for different system sizes. (b) The charge variance δS^{z^2} as a function of h for different system sizes on a log-lin scale. Here, $J^\perp = \Delta = 1$, $J^z = 1$, and the results are averaged over 200 samples. [(c) and (d)] Same as (b) and (c), but with $h = 7$ fixed and J^z varied. (e) Two-dimensional phase diagram of h and J^z . The blue region represents extensive charge fluctuation and is labeled as “Fluctuating charge”. The gray region represents negligible charge fluctuation and is labeled as “Frozen charge”.

In the numerical study, we prepare a randomly filled product state with half the spins up and half the spins down and compute $\delta S^{z^2}(t = 2L)$ as a function of h . Results for different system sizes L are shown in Fig. 3(a)-(d). When $J^z = 1$ is fixed, the charge fluctuation is extensive for $-5 \lesssim h \lesssim 5$ and negligible outside this range [Fig. 3(a) and Fig. 3(b)]. Note that in Fig. 3(a), the curve for $L = 8$ does not collapse with the other three lines, likely due to strong finite-size effects. When $h = 7$ is fixed, the charge fluctuation is negligible for $-2 \lesssim J^z \lesssim 2$ and extensive outside this range [Fig. 3(c) and Fig. 3(d)]. Based on the trend of the curve, it is likely that the system will re-enter into the charge-frozen phase when $|J^z| > 5$. However, due to system size limitations, precisely determining the phases in this range is challenging, so we do not present results for this region. We also extract a two-dimensional phase diagram by varying h and J^z , as shown in Fig. 3(e).

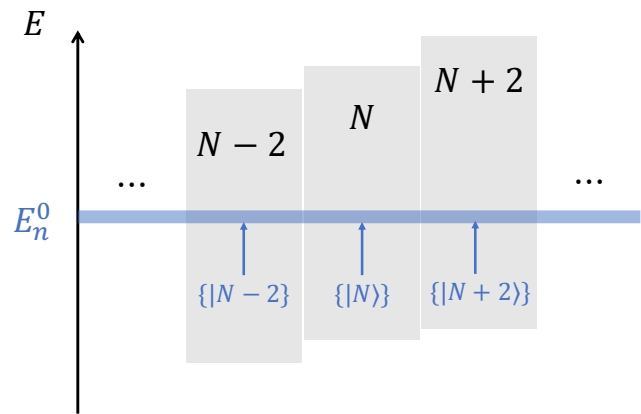


FIG. 4. Part of the many-body spectrum of \hat{H}_0 of free-fermion chain. The shaded gray area represents eigenstates that share the same labeled particle number: $N - 2$, N , or $N + 2$. E_n^0 is one particular eigenvalue of \hat{H}_0 .

V. EFFECTIVE HAMILTONIAN

The numerical simulation above suggests that by varying the bulk parameter, the boundary term may induce a bulk phase transition. To better understand this behavior, we employ perturbation theory. Note that the boundary term is supported on a finite number of sites and can only change the total energy by an $O(1)$ constant. Therefore in the perturbation framework, we can restrict our focus to the original eigenstates of \hat{H}_0 with a fixed energy E_0 and construct the effective Hamiltonian within this subspace. We then analyze the eigenstates of this effective Hamiltonian. Below, we start with the free-fermion chain and generalize this to the interacting system.

Consider a typical eigenstate $|n^0\rangle$ of \hat{H}_0 with energy E_n^0 and particle number N :

$$|n^0\rangle = \hat{c}_{k_1}^\dagger \hat{c}_{k_2}^\dagger \cdots \hat{c}_{k_N}^\dagger |0\rangle, k_1 < k_2 < \cdots < k_N. \quad (12)$$

For a typical $|n^0\rangle$, it is possible to construct other eigenstates with the same energy. These eigenstates can have particle numbers ranging from $N - \mathcal{O}(L)$ to $N + \mathcal{O}(L)$. We denote these eigenstates as $\{|N_1 \equiv N - \mathcal{O}(L)\rangle, \dots, \{|N\rangle, \dots, \{|N_2 \equiv N + \mathcal{O}(L)\rangle\}$, as illustrated in Fig. 4, which provides a schematic representation of the spectrum of \hat{H}_0 . Here, $\{|M\rangle\}$ indicates a set of states with energy E_n^0 and particle number M , while $|M\rangle_j$ refers to a specific state within $\{|M\rangle\}$, where the subscript j denotes the j -th state. The boundary term can couple sectors $\{|M\rangle\}$ with the same energy but different number of particles. In addition, these sectors need to have the same parity. Therefore, we focus on sectors with particle numbers that share the same parity as N , and we assume that N_1 and N_2 also have the same parity as N . To understand the properties of the perturbed state, we employ degenerate perturbation theory and construct the effective Hamiltonian \hat{H}_{eff}

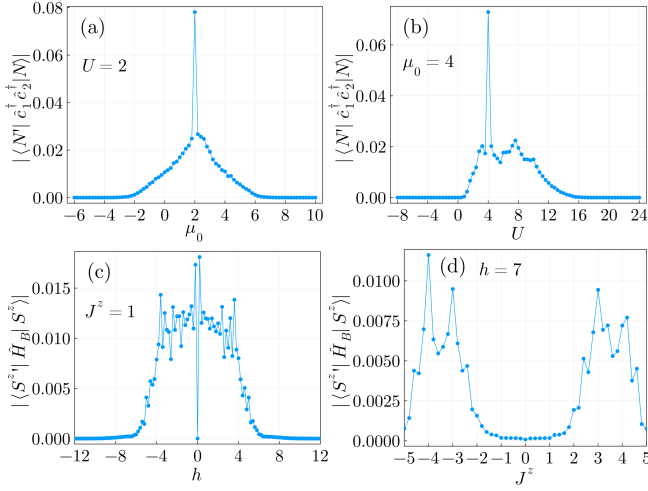


FIG. 5. The structure of $\hat{P}\hat{H}\hat{P}$. Interacting fermionic chain: (a) The absolute value of the inner product between $\hat{c}_1^\dagger \hat{c}_2^\dagger |N\rangle$ and $|N'\rangle$ for different values of μ_0 . Here, $L = 12$, $t_0 = \Delta = 1$, $U = 2$, and the results are averaged over 1000 pairs of eigenstates with an energy difference smaller than 0.1, satisfying $|N' - N - 2| < 0.00001$. [Corresponding to Fig. 2(a) and Fig. 2(b)]. (b) Same as (a), but with $\mu_0 = 4$ fixed and U varied. [Corresponding to Fig. 2(c) and Fig. 2(d)]. Interacting spin chain: (c) The absolute value of the inner product between $\hat{H}_B |S^z\rangle$ and $|S^{z'}\rangle$ for different values of h . Here, $L = 12$, $J^\perp = \Delta = 1$, $J^z = 1$, and the results are averaged over 1000 pairs of eigenstates with an energy difference smaller than 0.3, satisfying $|S^{z'} - S^z - 1| < 0.005$ or $|S^{z'} - S^z + 1| < 0.005$. [Corresponding to Fig. 3(a) and Fig. 3(b)]. (d) Same as (c), but with $h = 7$ fixed and J^z varied. [Corresponding to Fig. 3(c) and Fig. 3(d)].

within this subspace with energy E_0 [11]

$$\hat{H}_{\text{eff}}(E) = \hat{P}\hat{H}\hat{P} + \hat{P}\hat{H}\hat{Q} \frac{1}{E - \hat{Q}\hat{H}\hat{Q}} \hat{Q}\hat{H}\hat{P}, \quad (13)$$

where \hat{P} is the projector onto the subspace,

$$\hat{P} = \sum_{M=N_1}^{N_2} \sum_j |M\rangle_j \langle M|_j, \quad (14)$$

and $\hat{Q} = 1 - \hat{P}$. Suppose $\hat{H}|\Psi\rangle = E|\Psi\rangle$ in the full Hilbert space. Then, in the subspace projected by \hat{P} , we have $\hat{H}_{\text{eff}}(E)(\hat{P}|\Psi\rangle) = E(\hat{P}|\Psi\rangle)$.

In the following analysis, we focus on the first term of Eq. (13) and neglect the higher-order corrections from the second term. We find that considering only the first term is sufficient to explain the two distinct phases observed in the numerical simulations above. The first term $\hat{P}\hat{H}\hat{P}$ has diagonal elements given by E_n^0 ,

$$\begin{aligned} & \langle M | \hat{P}\hat{H}\hat{P} | M \rangle \\ &= \langle M | \hat{H} | M \rangle \\ &= \langle M | (\hat{H}_0 + \hat{H}_B) | M \rangle \\ &= \langle M | \hat{H}_0 | M \rangle = E_n^0. \end{aligned} \quad (15)$$

Since \hat{H}_B can only change two particles, the nonzero off-diagonal terms occur between sectors where the particle number differs by two. Specifically, consider $\langle M+2 | \hat{P}\hat{H}\hat{P} | M \rangle$,

$$\begin{aligned} & \langle M+2 | \hat{P}\hat{H}\hat{P} | M \rangle \\ &= \langle M+2 | \hat{H} | M \rangle \\ &= \langle M+2 | (\hat{H}_0 + \hat{H}_B) | M \rangle \\ &= \langle M+2 | \hat{H}_B | M \rangle \\ &= \frac{\Delta}{L} \sum_{k_1 k_2} e^{-i(k_1+2k_2)} \langle M+2 | \hat{c}_{k_1}^\dagger \hat{c}_{k_2}^\dagger | M \rangle. \end{aligned} \quad (16)$$

When $|\mu_0| > 2t_0$, there is a spectral gap for the quasiparticles, and the energies of the states $\hat{c}_{k_1}^\dagger \hat{c}_{k_2}^\dagger |M\rangle$ and $|M+2\rangle$ can never be equal. Consequently, \hat{H}_B cannot connect different sectors with the same energy and $\langle M+2 | \hat{P}\hat{H}\hat{P} | M \rangle$ vanishes, indicating that $\hat{P}\hat{H}\hat{P}$ is purely a *diagonal* matrix. However, when the gap closes, it becomes possible to construct a state $|M+2\rangle$ with the same energy as $\hat{c}_{k_1}^\dagger \hat{c}_{k_2}^\dagger |M\rangle$, leading to $\langle M+2 | \hat{P}\hat{H}\hat{P} | M \rangle \sim \mathcal{O}(\Delta/L)$. Therefore we obtain

$$\hat{P}\hat{H}\hat{P} = \begin{matrix} \{N_1\} \\ \{N_1+2\} \\ \{N_1+4\} \\ \vdots \\ \{N_2\} \end{matrix} \begin{pmatrix} E_n^0 & \mathcal{O}(\Delta/L) & \mathcal{O}(\Delta/L) & \dots & \mathcal{O}(\Delta/L) \\ \mathcal{O}(\Delta/L) & E_n^0 & \mathcal{O}(\Delta/L) & \dots & \mathcal{O}(\Delta/L) \\ \mathcal{O}(\Delta/L) & \mathcal{O}(\Delta/L) & E_n^0 & \dots & \mathcal{O}(\Delta/L) \\ \vdots & \vdots & \vdots & \ddots & \vdots \\ \mathcal{O}(\Delta/L) & \mathcal{O}(\Delta/L) & \mathcal{O}(\Delta/L) & \dots & E_n^0 \end{pmatrix}. \quad (17)$$

Consequently, the eigenstates become superpositions of states with different particle numbers and with extensive charge fluctuations. This leads to a simple *pumping picture*: the spectral gap of the quasiparticle disfavors the boundary from pumping a particle into the bulk. However, when the gap disappears, the pumping process is not suppressed, and the final state can have a very different particle number. In Appendix D, we consider a one-dimensional free-fermion chain divided into two half-chains and study particle transport between them, which can also be analyzed using the simple pumping picture.

We observe that whether $\hat{P}\hat{H}\hat{P}$ is a purely diagonal matrix serves as a criterion for the phase transition. When $\langle M+2 | \hat{P}\hat{H}\hat{P} | M \rangle = 0$, the charge cannot be pumped into the system and different charge sectors remain disconnected, indicating the charge-frozen phase. Notably, the second term in Eq. (13) can, in principle, establish connections between sectors of the same energy with particle numbers differing by $\mathcal{O}(L)$, which is reflected in the nonzero off-diagonal elements in the effective Hamiltonian. However, this process requires applying \hat{H}_B many times and is therefore highly suppressed. Consequently, we neglect this term and consider only $\hat{P}\hat{H}\hat{P}$ in our analysis, which we believe is sufficient to capture the essential physics of the transition, although this has not been rigorously proven in this paper.

We can examine this criterion in the context of generic models: consider the unperturbed Hamiltonian \hat{H}_0 and

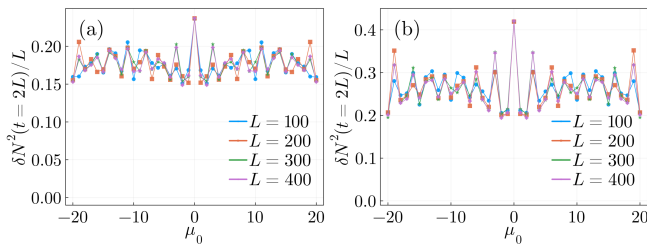


FIG. 6. Floquet systems. (a) Energy conservation is broken. The density of charge variance $\delta N^2/L$ as a function of μ_0 for different system sizes. Here, $t_0 = \Delta = 1$, $\nu = 0.5$, and the results are averaged over 1000 samples. (b) Energy conservation is replaced by conservation of spin in the z-direction in the spinful model. The density of charge variance $\delta N^2/L$ as a function of μ_0 for different system sizes. Here, $t_0 = \Delta = 1$, and the results are averaged over 1000 samples.

the charge operator \hat{O} , and find out the eigenstates of both \hat{H}_0 and \hat{O} with the same energy E_0 . We denote these eigenstates by their corresponding charges as $|O\rangle$. We then examine the effective Hamiltonian in the subspace spanned by these eigenstates, defined by the projector \hat{P} . In many cases, we believe it is sufficient to consider $\hat{P}\hat{H}\hat{P}$ alone. If the effective Hamiltonian allows different charge sectors to connect, the final state can exhibit extensive charge fluctuations. Conversely, if such connections are absent, the final state will exhibit negligible charge fluctuations. Specifically, for the previous two interacting models, we select an energy E_0 and identify all eigenstates of \hat{H}_0 with energies close to E_0 . Among them, we choose a pair of eigenstates, $|O\rangle$ and $|O'\rangle$, whose corresponding charges differ, and compute the matrix element $|\langle O'|\hat{H}_B|O\rangle|$. (To illustrate, in the interacting fermionic chain, we choose a pair of eigenstates with the same energy and a particle number difference of two: $|N\rangle$ and $|N+2\rangle$, since the boundary term can only change the particle number by two. We then test how the boundary term connects these two states by calculating the matrix element $|\langle N+2|\hat{H}_B|N\rangle|$.) As shown numerically in Fig. 5, this matrix element undergoes significant variation as the bulk parameter changes. For example, in Fig. 5(a) for the interacting fermionic chain with $U = 2$ fixed, it is nonzero in the range $-2 \lesssim \mu_0 \lesssim 6$, indicating that $\hat{P}\hat{H}\hat{P}$ contains nonzero off-diagonal elements, whereas outside this range, it is nearly zero, indicating that $\hat{P}\hat{H}\hat{P}$ can be effectively approximated as a diagonal matrix. These results are consistent with the observed charge fluctuation behavior in Fig. 2(a) and Fig. 2(b).

VI. BOUNDARY PERTURBATION ON FLOQUET SYSTEMS

One question that arises is whether the results would still hold if the energy conservation law is broken or replaced by a different conservation law. In this section, we present numerical results for the two cases. In both cases,

we observe that the charge-frozen phase disappears.

In Floquet systems, where systems are driven periodically, energy conservation law is broken. Specifically, we consider a simple model derived from the free-fermion chain: We prepare a randomly filled product state with a filling factor ν and evolve the state periodically

$$|\Psi(t)\rangle = (e^{-i\hat{H}_B} e^{-i\hat{H}_0})^{t/2} |\Psi(0)\rangle, \quad (18)$$

where \hat{H}_0 and \hat{H}_B are defined in Eq. (1) and Eq. (3). The state is evolved for a long time and the steady-state value of δN^2 is computed as a function of μ_0 . The results for different systems sizes are shown in Fig. 6(a). Even when the absolute value of chemical potential μ_0 is as high as 20, the charge fluctuation remains extensive, indicating the disappearance of the charge-frozen phase.

Next, we replace the conservation of energy with the conservation of spin in the z-direction. Specifically, we consider the non-interacting spinful model: The bulk Hamiltonian is

$$\hat{H}_0 = \sum_{j,\sigma=\uparrow,\downarrow} t_0 (\hat{c}_{j,\sigma}^\dagger \hat{c}_{j+1,\sigma} + \hat{c}_{j+1,\sigma}^\dagger \hat{c}_{j,\sigma}) - \sum_{j,\sigma=\uparrow,\downarrow} \mu_0 \hat{n}_{j,\sigma}, \quad (19)$$

where $\sigma = \uparrow, \downarrow$ is the spin index. The boundary perturbation is

$$\hat{H}_B = \Delta (\hat{c}_{1,\uparrow}^\dagger \hat{c}_{2,\downarrow}^\dagger + \hat{c}_{2,\downarrow} \hat{c}_{1,\uparrow}). \quad (20)$$

Note that both \hat{H}_0 and \hat{H}_B commute with the spin operator in the z-direction $\hat{S}^z = \sum_j (\hat{n}_{j,\uparrow} - \hat{n}_{j,\downarrow})/2$ [12], whereas only \hat{H}_0 commutes with the number operator $\hat{N} = \sum_j (\hat{n}_{j,\uparrow} + \hat{n}_{j,\downarrow})$. We prepare a randomly filled product state with half the spins up and half the spins down and evolve the state periodically according to Eq. (18). The state is evolved for a long time and the steady-state value of δN^2 is computed as a function of μ_0 . The results for different system sizes are shown in Fig. 6(b). As in the previous case, the charge fluctuation remains extensive across a wide range of chemical potential values.

VII. DISCUSSION

In this paper, we investigate the impact of boundary perturbations on the dynamics of a Hamiltonian with an additional continuous symmetry. We numerically study both free and interacting models, demonstrate that if the boundary perturbation breaks this continuous symmetry, varying the bulk parameters can give rise to two distinct phases characterized by charge fluctuations: (1) Frozen phase: The charge fluctuation is negligible, and the boundary perturbation does not significantly influence the bulk dynamics. (2) Fluctuating phase: Extensive charge fluctuation occurs, allowing charges to be pumped into or out of the system through the boundary. Using degenerate perturbation theory, we provide an explanation for this behavior from a simple pumping

picture and propose a criterion for determining the phase diagram of a generic model. Furthermore, although our study focuses on one-dimensional models, our findings remain applicable in higher dimensions.

The energy conservation is a necessary condition for the existence of the phase transition. We demonstrate that when the energy conservation law is broken or replaced by a different conservation law, only a charge-fluctuating phase is observed, suggesting that energy conservation has unique effects.

In the future, it would be intriguing to investigate quantum systems with energy conservation alongside multiple other conservation laws, which may exhibit strong fragmentation behavior [13, 14]. Previous research has shown that introducing boundary perturbations can lead to ultraslow thermalization in such systems [15]. Ex-

ploring the potential transition to charge-frozen phases in these systems would be particularly interesting.

ACKNOWLEDGMENTS

We thank Vikram Ravindranath and Hanchen Liu for helpful discussions. Q.G. expresses gratitude to Vikram Ravindranath for his guidance on numerical simulations of Gaussian states. We gratefully acknowledge computing resources from Research Services at Boston College and the assistance provided by Wei Qiu. This research is supported by the National Science Foundation under Grant No. DMR-2219735 (Q.G. and X.C.).

-
- [1] J. Kondo, Resistance minimum in dilute magnetic alloys, *Progress of theoretical physics* **32**, 37 (1964).
 - [2] A. C. Hewson, *The Kondo problem to heavy fermions*, 2 (Cambridge university press, 1997).
 - [3] J. Cardy, Boundary conformal field theory, *arXiv preprint hep-th/0411189* (2004).
 - [4] N. Andrei, A. Bissi, M. Buican, J. Cardy, P. Dorey, N. Drukker, J. Erdmenger, D. Friedan, D. Fursaev, A. Konechny, *et al.*, Boundary and defect cft: open problems and applications, *Journal of Physics A: Mathematical and Theoretical* **53**, 453002 (2020).
 - [5] R. A. Blythe and M. R. Evans, Nonequilibrium steady states of matrix-product form: a solver’s guide, *Journal of Physics A: Mathematical and Theoretical* **40**, R333 (2007).
 - [6] G. T. Landi, D. Poletti, and G. Schaller, Nonequilibrium boundary-driven quantum systems: Models, methods, and properties, *Reviews of Modern Physics* **94**, 045006 (2022).
 - [7] Q. Gao, P. Zhang, and X. Chen, Information scrambling in free fermion systems with a sole interaction, *Physical Review B* **110**, 035137 (2024).
 - [8] Q. Gao, T. Zhou, P. Zhang, and X. Chen, Scrambling transition in free fermion systems induced by a single impurity, *arXiv preprint arXiv:2403.03457* (2024).
 - [9] S. Bravyi, Lagrangian representation for fermionic linear optics, *arXiv preprint quant-ph/0404180* (2004).
 - [10] V. Ravindranath, Z.-C. Yang, and X. Chen, Free fermions under adaptive quantum dynamics, *arXiv preprint arXiv:2306.16595* (2023).
 - [11] See, for example, Ref. [16]. Additionally, refer to Appendix C for the detailed derivation.
 - [12] H. Tasaki, *Physics and mathematics of quantum many-body systems*, Vol. 66 (Springer, 2020).
 - [13] P. Sala, T. Rakovszky, R. Verresen, M. Knap, and F. Pollmann, Ergodicity breaking arising from hilbert space fragmentation in dipole-conserving hamiltonians, *Physical Review X* **10**, 10.1103/physrevx.10.011047 (2020).
 - [14] S. Moudgalya and O. I. Motrunich, Hilbert space fragmentation and commutant algebras, *Physical Review X* **12**, 10.1103/physrevx.12.011050 (2022).
 - [15] Y. Han, X. Chen, and E. Lake, Exponentially slow thermalization and the robustness of hilbert space fragmentation (2024), *arXiv:2401.11294* [quant-ph].
 - [16] F. Mila and K. P. Schmidt, Strong-coupling expansion and effective hamiltonians, in *Introduction to Frustrated Magnetism: Materials, Experiments, Theory* (Springer, 2010) pp. 537–559.

Appendix A: Particle dynamics and energy dynamics of free-fermion chain

We consider the same free-fermion chain as in the manuscript:

$$\hat{H}_0 = \sum_{j=1}^L t_0 (\hat{c}_j^\dagger \hat{c}_{j+1} + \hat{c}_{j+1}^\dagger \hat{c}_j) - \sum_{j=1}^L \mu_0 \hat{n}_j, \quad (\text{A1})$$

$$\hat{H}_B = \Delta (\hat{c}_1^\dagger \hat{c}_2^\dagger + \hat{c}_2 \hat{c}_1).$$

We prepare a randomly chosen initial state $|\Psi(0)\rangle$ with a fixed filling factor $\nu \neq 0$, so that $N = L\nu$:

$$\hat{N} |\Psi(0)\rangle = L\nu |\Psi(0)\rangle. \quad (\text{A2})$$

To examine how the boundary term \hat{H}_B influences the energy of the system, we first evolve the state unitarily with \hat{H}_0 from time $t = 0$ to $t = L$. Then, we add the boundary term and continue the unitary evolution with $\hat{H} = \hat{H}_0 + \hat{H}_B$ from time $t = L$ to $t = 2L$, tracking the energy dynamics throughout. Specifically, the energy of the system from time $t = 0$ to $t = L$ is given by $E(t) = \langle \Psi(t) | \hat{H}_0 | \Psi(t) \rangle$, and from time $t = L$ to $t = 2L$, the energy is $E(t) = \langle \Psi(t) | \hat{H} | \Psi(t) \rangle$. We present the particle dynamics and energy dynamics for two examples in different phases in Fig. A1. In both phases, the energy remains constant, as the expectation value of the boundary term for a particle-conserving state is zero. However, the particle number undergoes a significant change when the spectral gap disappears, while it remains constant when the spectral gap is present.

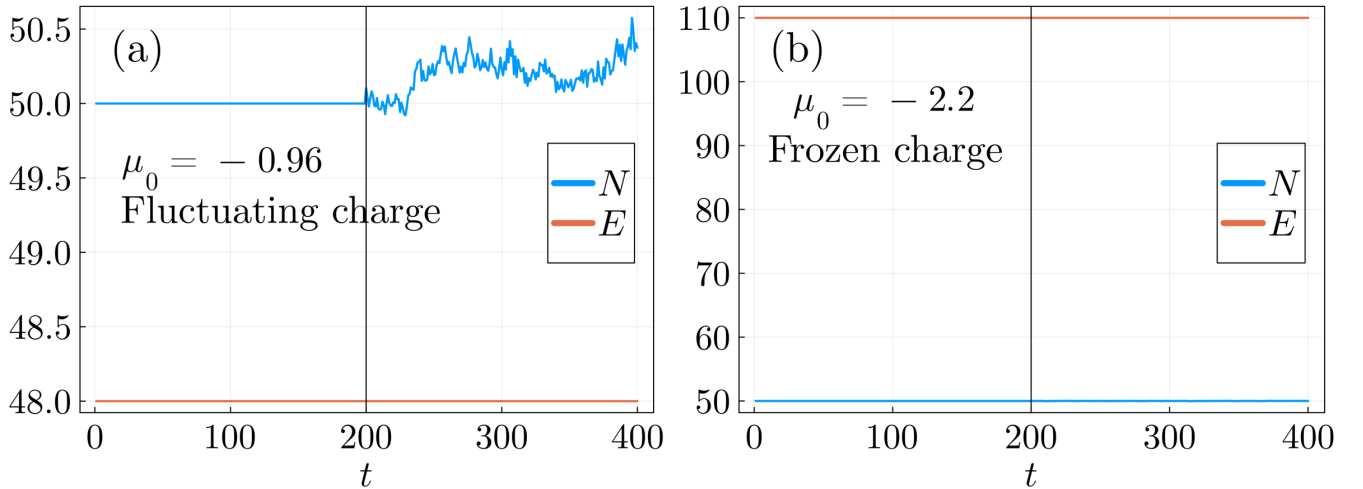


FIG. A1. Free-fermion chain. The particle dynamics and energy dynamics for (a) $\mu_0 = -0.96$ and (b) $\mu_0 = -2.2$. The black vertical lines in both figures indicate the moment when the boundary term is added. Here, $t_0 = \Delta = 1$, $\nu = 0.5$, and $L = 100$.

Appendix B: Interacting fermionic chain with a filling factor $\nu = 0.25$

In this section, we present the results shown in Fig. A2 for the interacting model with a filling factor $\nu = 0.25$, in comparison to $\nu = 0.5$ discussed in the main manuscript. The two results demonstrate that the transition is independent of the filling factor in this model.

Appendix C: Derivation of the effective Hamiltonian

Suppose $\hat{H} |\Psi\rangle = E |\Psi\rangle$, and the full Hilbert space of the system can be decomposed into two orthogonal subspaces, with \hat{P} and \hat{Q} as the corresponding projectors, satisfying $\hat{P} + \hat{Q} = 1$. Our goal is to derive the effective Hamiltonian in the subspace projected by \hat{P} .

Since $\hat{P} + \hat{Q} = 1$, we can rewrite the Schrodinger equation as:

$$\hat{H}(\hat{P} + \hat{Q}) |\Psi\rangle = E(\hat{P} + \hat{Q}) |\Psi\rangle. \quad (\text{A1})$$

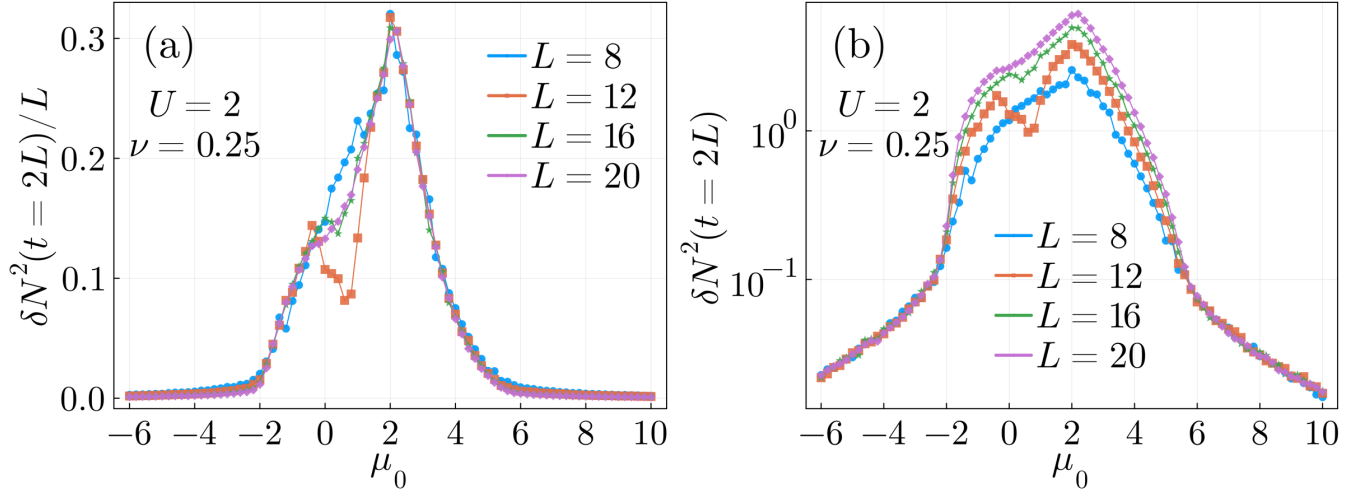


FIG. A2. Interacting fermionic chain. (a) The density of charge fluctuation $\delta N^2/L$ as a function of μ_0 for different system sizes. (b) The charge fluctuation δN^2 as a function of μ_0 for different system sizes on a log-lin scale. Here, $t_0 = \Delta = 1$, $U = 2$, $\nu = 0.25$, and the results are averaged over 200 samples.

By projecting separately with \hat{P} and \hat{Q} , we obtain:

$$\hat{P}\hat{H}\hat{P}|\Psi\rangle + \hat{P}\hat{H}\hat{Q}|\Psi\rangle = E\hat{P}|\Psi\rangle, \quad (\text{A2})$$

$$\hat{Q}\hat{H}\hat{P}|\Psi\rangle + \hat{Q}\hat{H}\hat{Q}|\Psi\rangle = E\hat{Q}|\Psi\rangle, \quad (\text{A3})$$

and

$$\begin{aligned} (\text{A3}) &\implies \hat{Q}\hat{H}\hat{P}|\Psi\rangle = E\hat{Q}|\Psi\rangle - \hat{Q}\hat{H}\hat{Q}\hat{Q}|\Psi\rangle = (E - \hat{Q}\hat{H}\hat{Q})\hat{Q}|\Psi\rangle \\ &\implies \hat{Q}|\Psi\rangle = (E - \hat{Q}\hat{H}\hat{Q})^{-1}\hat{Q}\hat{H}\hat{P}|\Psi\rangle, \\ (\text{A2}) &\implies \hat{P}\hat{H}\hat{P}|\Psi\rangle + \hat{P}\hat{H}\hat{Q}\hat{Q}|\Psi\rangle = E\hat{P}|\Psi\rangle \\ &\implies \hat{P}\hat{H}\hat{P}|\Psi\rangle + \hat{P}\hat{H}\hat{Q}(E - \hat{Q}\hat{H}\hat{Q})^{-1}\hat{Q}\hat{H}\hat{P}|\Psi\rangle = E\hat{P}|\Psi\rangle \\ &\implies \left(\hat{P}\hat{H}\hat{P} + \hat{P}\hat{H}\hat{Q}(E - \hat{Q}\hat{H}\hat{Q})^{-1}\hat{Q}\hat{H}\hat{P}\right)\left(\hat{P}|\Psi\rangle\right) = E\left(\hat{P}|\Psi\rangle\right). \end{aligned} \quad (\text{A4})$$

The effective Hamiltonian in the subspace projected by \hat{P} is

$$\hat{H}_{\text{eff}}(E) = \hat{P}\hat{H}\hat{P} + \hat{P}\hat{H}\hat{Q}(E - \hat{Q}\hat{H}\hat{Q})^{-1}\hat{Q}\hat{H}\hat{P}. \quad (\text{A5})$$

Appendix D: Particle transport in a free-fermion chain

The gap in the bulk spectrum can also influence the transport from other systems. We consider the Hamiltonian of a one-dimensional free-fermion chain of finite size L with open boundary conditions:

$$\begin{aligned} \hat{H}_0 &= \hat{H}_l + \hat{H}_r, \\ \hat{H}_l &= \sum_{j \in l} t_l (\hat{c}_j^\dagger \hat{c}_{j+1} + \hat{c}_{j+1}^\dagger \hat{c}_j) - \sum_{j \in l} \mu_l \hat{n}_j, \\ \hat{H}_r &= \sum_{j \in r} t_r (\hat{c}_j^\dagger \hat{c}_{j+1} + \hat{c}_{j+1}^\dagger \hat{c}_j) - \sum_{j \in r} \mu_r \hat{n}_j. \end{aligned} \quad (\text{A1})$$

Here, the system is divided into two half-chains, with the subscript l and r denoting the left and right parts. Note that \hat{H}_0 commutes with the number operator of the right part, $\hat{N}_r = \sum_{j \in r} \hat{n}_j$. Initially, we fill the left part with a filling factor ν_l and the right part with a filling factor ν_r . We add a coupling term \hat{H}_C between the left and right parts:

$$\hat{H}_C = \Delta (\hat{c}_{L/2}^\dagger \hat{c}_{L/2+1} + \hat{c}_{L/2+1}^\dagger \hat{c}_{L/2}). \quad (\text{A2})$$

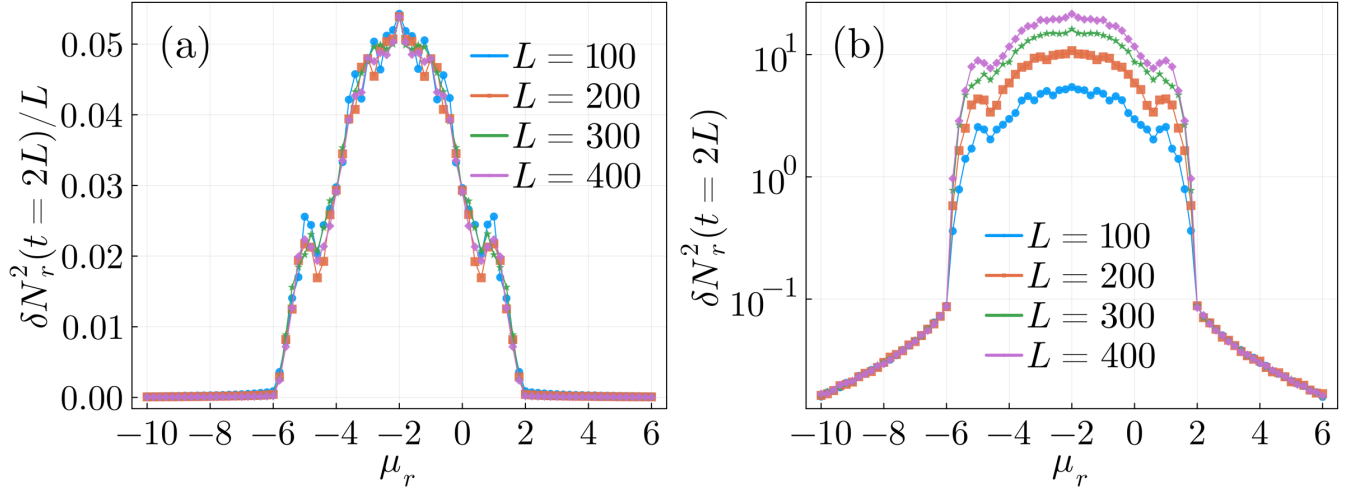


FIG. A3. Transport in a free-fermion chain. (a) The density of charge fluctuation $\delta N_r^2/L$ as a function of μ_r for different system sizes. (b) The charge fluctuation δN_r^2 as a function of μ_r for different system sizes on a log-lin scale. Here, $t_l = t_r = \Delta = 1$, $\mu_l = -2$, $\nu_l = 0.5$, $\nu_r = 0.25$, and the results are averaged over 1000 samples.

We evolve the system unitarily with $\hat{H} = \hat{H}_0 + \hat{H}_C$ for a long time. Since \hat{H} does not commute with \hat{N}_r , the particle number N_r can change over time. To study *how the left part influences the originally conserved particle number in the right part*, we calculate the charge variance of the right part,

$$\delta N_r^2(t) = \langle \Psi(t) | (\hat{N}_r - \langle \Psi(t) | \hat{N}_r | \Psi(t) \rangle)^2 | \Psi(t) \rangle. \quad (\text{A3})$$

The results for different system sizes L are presented in Fig. A3. These results can be understood as follows: for eigenstates of \hat{H}_0 with the same total particle number but different particle numbers in the right part, N_r and $N_r + 1$, the energy difference is

$$\begin{aligned} & - (2t_l \cos k_l - \mu_l) + (2t_r \cos k_r - \mu_r) \\ & = (-2t_l \cos k_l + 2t_r \cos k_r) + (\mu_l - \mu_r) \\ & \in [-2(|t_l| + |t_r|) + (\mu_l - \mu_r), 2(|t_l| + |t_r|) + (\mu_l - \mu_r)]. \end{aligned} \quad (\text{A4})$$

When $\mu_r < -2(|t_l| + |t_r|) + \mu_l$ or $\mu_r > 2(|t_l| + |t_r|) + \mu_l$, the energy gap for a single pump exists, and particle transport from the left part cannot influence the particle number of the right part in the thermodynamic limit.